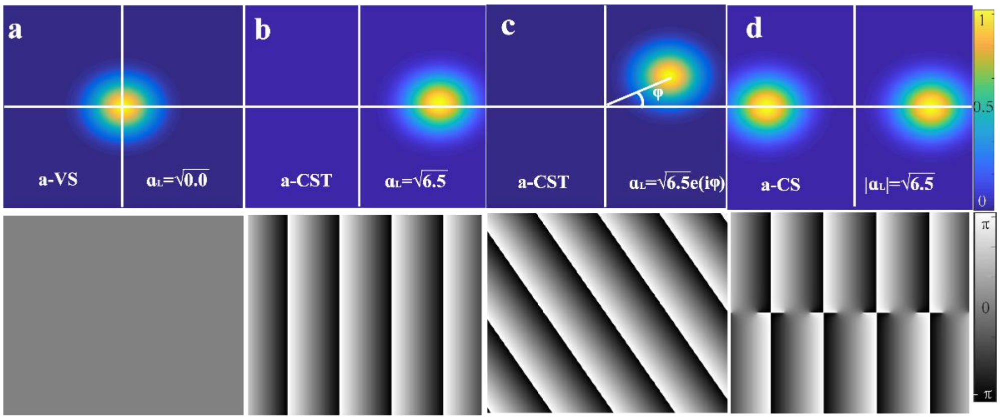

Supplementary Figure 1: Intensity and phase distributions for the orbital angular momentum (OAM) states. a-d: Intensity distributions for the analogous vacuum state (a-VS), coherent state (a-CST), rotated coherent state, and cat state (a-CS), respectively. Four subfigures at the bottom of panel a-d are the corresponding phase hologram for generations in spatial light modulation (z=0). In the simulation, the wavelength and waist are 780 nm and 200 um; α_L represents the size of the a-CST; and ϕ is the phase factor of the a-CST.

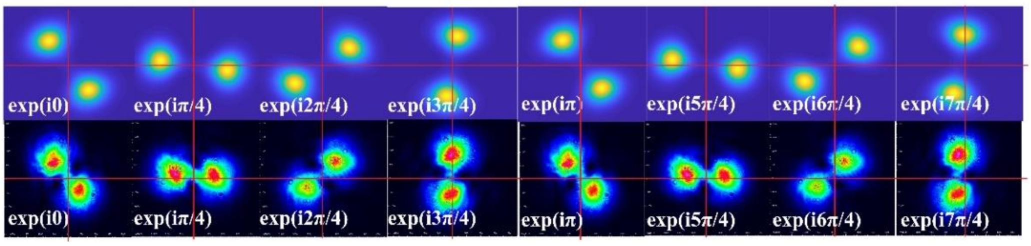

Supplementary Figure 2: Theoretical (the top panels) and experimental (the bottom panels) results of rotations for the analogous cat state. The position of the charge coupled device (CCD) camera is placed ~ 1 m behind the beam splitter (see Fig. 2 in the main text).

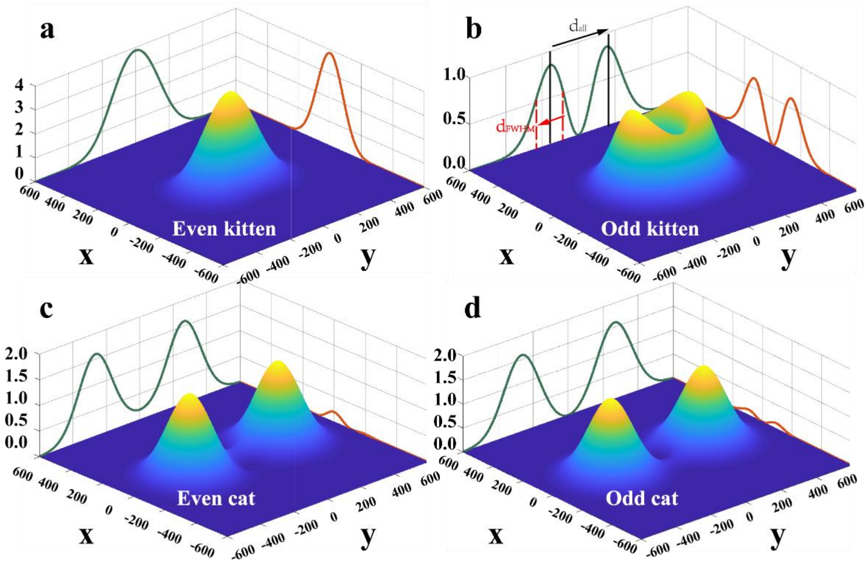

Supplementary Figure 3: Intensity distributions for an even (a) and odd (b) "kitten" states ($|\alpha_L| = \sqrt{0.5}$). Panels c and d show the intensity distribution for an even (c) and odd (d) "cat" states ($|\alpha_L| = \sqrt{3.5}$). $|\alpha_L|$ represents the size of the a-CS.

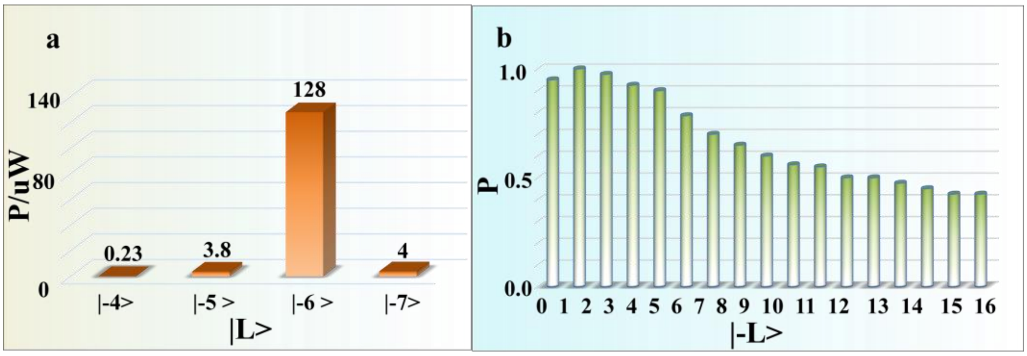

Supplementary Figure 4: Intensity distributions for the orbital angular momentum (OAM) superposition states. a: the mode-orthogonality for the OAM eigenstate $|6\rangle$, where the *x*-axis is the conjugate OAM eigenstate; and the *y*-axis is the power with the unit μW. b: Normalized intensity distributions for an OAM superposition state with 17 modes.

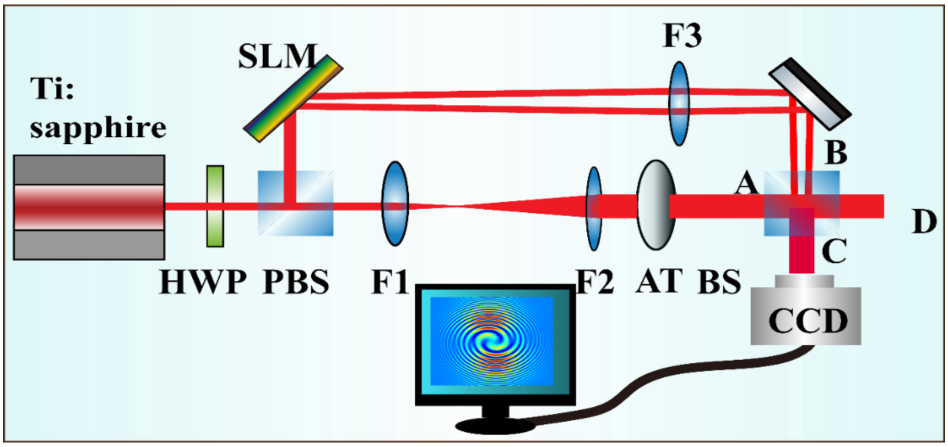

Supplementary Figure 5: The experimental setup for implementing interference between a plane wave and an analogous cat state. HWP: half wave plate; AT: neural attenuator; SLM: spatial light modulator. F1, F2, and F3: the convex lens of focal length 75 mm, 200 mm, and 125 mm.

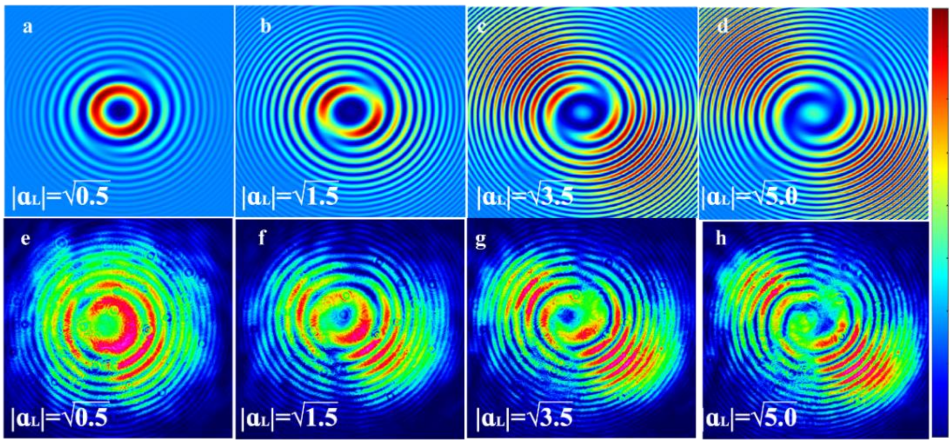

Supplementary Figure 6: Interference patterns between a plane wave and the analogous cat states (a-CS). a-d: the theoretical simulations for the a-CS from "kitten" to "cat" states based on Eq. 6 in the main text. e-h: the experimental interference patterns acquired by a charge coupled device (CCD) camera.

$\lvert\alpha_L\rvert^2$	0.5	1.5	2.5	3.5	5.0
r	0.5794	0.2014	0.0704	0.0226	6.8*10^-4

Supplementary Table 1: Overlaps between two analogous coherent states with opposite-amplitude.

Supplementary Note 1. Definition of analogous cat states and fundamental characteristics.

The normalized orbital angular momentum (OAM)-eigenstate associated with the Laguerre–Gaussian (LG) mode can be represented as $\langle Cylin(r,\phi,z)|L\rangle \to LG_p^l(\rho,\phi,z)$ in the cylindrical representation. Without the radial index *p*, it takes the form [1].

$$\langle Cylin(r,\phi,z)|L\rangle=\sqrt{\frac{2}{\pi|L!|}}\frac{1}{w(z)}\left(\frac{\sqrt{2}r}{w(z)}\right)^{|l|}\cdot\exp\left(-\frac{r^2}{w(z)^2}+i\left(L\phi-\frac{kr^2z}{2(z^2+z_r^2)}+(|L|+1)a\tan\left(\frac{z}{z_r}\right)\right)\right) \quad \text{(S1)}$$

The analogous cat state (a-CS) $|\alpha_L\rangle+|-\alpha_L\rangle$ is a superposition of two analogous coherent states (a-CST). One of them, i.e., $|\alpha_L\rangle$, is a weighted superposition of each OAM eigenstate which given in Eq. 1 in the main text. Inserting it into Eq. S1, we obtain the expression of the a-CST in the cylindrical representation along the propagating direction *z*:

$$\begin{aligned}\langle Cylin(r,\phi,z)|\alpha_L\rangle&=C(z)\cdot\exp\left(-\frac{r^2}{w(z)^2}\right)\cdot\exp\left(\alpha_L\frac{\sqrt{2}r}{w(z)}\exp\left(i\left(\phi+\tan^{-1}\left(\frac{z}{z_r}\right)\right)\right)\right)\\&=\sqrt{\frac{2}{\pi}}\frac{1}{w(z)}\exp\left(-\frac{|\alpha_L|^2}{2}-i\frac{kr^2z}{2(z^2+z_r^2)}+i\tan^{-1}\left(\frac{z}{z_r}\right)\right)\cdot\exp\left(-\frac{r^2}{w(z)^2}\right)\cdot\exp\left(\alpha_L\frac{\sqrt{2}r}{w(z)}\exp\left(i\left(\phi+\tan^{-1}\left(\frac{z}{z_r}\right)\right)\right)\right)\end{aligned} \quad \text{(S2)}$$

Here, $\alpha_L(=|\alpha_L|e^{i\varphi})$ is a complex number giving the position of the a-CST in cylindrical coordinates; $|\alpha_L|$ is the radial distance between the center of the a-CST and the analogous vacuum state (a-VS, $|0\rangle$, Gaussian beam); and φ defines the rotation angle along the horizontal axis. In Eq. S2, the imaginary part like an optical grating, represents a displacement operation moving an a-VS to a-CST. The dynamic movement is similar to the displacement operation on the usual coherent state.

In the cylindrical representation, the a-CS could be written as $\langle C|\alpha_L\rangle+e^{i\theta}\langle C|-\alpha_L\rangle$. The intensity of the a-CS gives the following form,

$$\begin{aligned}|\langle Cylin(r,\phi,z)|Cat\rangle|^2&=|\langle C|\alpha_L\rangle|^2+|\langle C|-\alpha_L\rangle|^2+2\cos(\theta-2\alpha_L\sin(\Phi))|\langle C|0\rangle|^2\\&=G(\alpha_L)+G(-\alpha_L)+2\cos(\theta-2\alpha_L\sin(\Phi))\cdot G(0)\end{aligned} \quad \text{(S3)}$$

Where $\alpha(=\sqrt{2}\alpha_L r/w_0)$ and $\Phi(=\phi+\tan^{-1}(z/z_r))$ are the size and phase constants of the a-CS, respectively; $G(0)$ describes the a-VS $C(z)\cdot\exp(-r^2/w(z)^2)$; $G(\pm\alpha_L)$ represent two Gaussian intensity lobes (GILs), and the last term gives the interference between them. The intensity distribution of an a-CS is similar to the Wigner function of the optical cat state in phase space [2-4].

Supplementary Figure 1 shows intensity-distribution of the a-VS, a-CST, the rotated a-CST, and a-CS, respectively, where the size of an a-CS is $|\sqrt{6.5}|$. Correspondingly, the phase holograms show different operations on the input state (a-VS). Supplementary Movies 1 shows the dynamic intensity- distribution of an odd a-CS with size from 0 to $\sqrt{8}$, and Supplementary Movies 2 shows the situation of the interference between "alive" and "dead" cat state ($|\alpha_L|=1.0$). Experimentally, the a-CS can be created by loading these holograms.

In the observed plane, the position of the a-CS depends on $\alpha_L(=|\alpha_L|e^{i\varphi})$, where φ is the rotational angle. The theoretical and experimental results of rotations are shown in Supplementary Figure 2, where the size is $|\alpha_L|=\sqrt{2.5}$; and the phase φ takes $0,\pi/4,2\pi/4,...7\pi/4$ for each of eight panels. Because the GILs of the a-CS would have a relative rotation in the observed plane, we add a basic phase of around 1.2π/4 for a better comparison with experimental results.

Supplementary Note 2. The "Macroscopicity" of the a-CS.

Supplementary Figure 3 shows the three-dimensional intensity distributions of an even (odd) "kitten" ($|\alpha_L|=\sqrt{0.5}$) and "cat" ($|\alpha_L|=\sqrt{3.5}$), respectively. In these panels, the green and red lines on the marginal planes show the tangential distributions along x=0 and y=0. As the cat state grows, the distance between two GILs increases. Therefore, one can define a "Macroscopicity" of an a-CS based on the movement.

The movement d is the center distance between an a-CST and a-VS, which is derived by solving the equation $\partial|\langle Cylin(r,\phi,z)|\alpha_L\rangle|^2/\partial r=0$,

$$d=\frac{\sqrt{2}\alpha}{2}w(z)=\frac{\sqrt{2}\alpha}{2}w_0\sqrt{1+\left(\frac{z}{z_r}\right)^2} \tag{S4}$$

In Eq. S4, the movement d is proportional to the size of the a-CST. Furthermore, the relative movement is not dependent on distance z, which indicates that one could detect it in any position. Be analogous to the "Macroscopicity" criterion in Ref. [5]; we define a criterion M as follows:

$$M=\frac{\theta_{\sin g}}{\theta_{suo}}\approx\frac{d_{All}}{d_{FWHM}}=\frac{\frac{\sqrt{2}}{2}|\alpha|w_0\sqrt{1+\left(\frac{z}{z_r}\right)^2}}{w_0\sqrt{1+\left(\frac{z}{z_r}\right)^2}}=\frac{\sqrt{2}}{2}|\alpha| \tag{S5}$$

where d_{all} and d_{FWHM} represent the distance (see Supplementary Figure 3b) that we only consider the odd cat state. Usually, two spatially localized Gaussian intensity packets can be merely generated by a beam splitter, which is the very particular situation of the state prepared in our setup. The intensity distribution of an a-CS in Eq. S3 includes three parts, two spatial localized Gaussian intensity lobes $G(\pm\alpha_L)$, and the interference term. The interference depends on the size of the cat state, the vortex related phase Φ, and the global phase factor θ. All of the parameters create a cat state that can be of movement, rotation, and interference in the Bloch sphere. However, it is difficult to realize such a state by a beam splitter. For a Gaussian beam passing through a beam splitter, the transmission intensity distribution should have only two terms, $I=R\cdot G_R+T\cdot G_T$. Experimentally, the perfect and arbitrary coherent superposition state in the Bloch sphere is difficult to realize by only one beam splitter, although the interference can be created with the help of other elements, such as MZ-interferometer.

Supplementary Note 3. Mode orthogonality and Interference in the Bloch-sphere.

In this section, we study the interference in the Bloch-sphere. For an OAM superposition state of $|\psi\rangle=\alpha|L_1\rangle+\beta|L_2\rangle$, there exists an ideal conjugated unit transform:

$$\langle\psi|\psi\rangle=\alpha^2\langle L_1|L_1\rangle+\beta^2\langle L_2|L_2\rangle+\alpha^+\beta\langle L_1|L_2\rangle+\alpha\beta^+\langle L_1|L_2\rangle=\alpha^2+\beta^2 \tag{S6}$$

Experimentally, one can perform projection measurement with the help of SLM and a single mode fiber, which can be expressed as $|-L\rangle \to \langle L|$. Therefore, the corresponding transform is:

$$\langle \psi | \psi \rangle \to \mathrm{U}_{SLM} \cdot |\psi\rangle = \alpha^2 |0\rangle + \beta^2 |0\rangle + \alpha\beta |L_1 - L_2\rangle + \beta\alpha |L_2 - L_1\rangle \tag{S7}$$

Where $\mathrm{U}_{SLM}\left(= \alpha|-L_1\rangle + \beta|-L_2\rangle\right)$ is the corresponding measured phase loaded on the SLM; $\left|\langle \psi | \psi \rangle\right|^2$ is proportional to the detected power. Supplementary Figure 4a presents the mode-orthogonality of the single OAM eigenstate $|6\rangle$. For the single OAM eigenstate $|6\rangle$, the crosstalk is very weak (32:1), which indicates that the OAM mode-orthogonality is reliable. Supplementary Figure. 4b shows the spatial mode distribution for OAM separated superposition state $|0\rangle + |1\rangle + |2\rangle + ... + |16\rangle$. The results illustrate that the collection efficiency decreases as the topologic charge L increases, which give rise to a low similarity (fidelity) during the state tomography.

Because the a-CS is a superposition of infinate OAM eigenstates, the conjugated transform of the a-CS can be written as $\left|\langle \alpha_L | \alpha_L^{'} \rangle\right|^2 = \exp\left(-|\alpha - \alpha'|^2\right)$. Based on this equation, one can calculate the corresponding transforms for even and odd analogous cats.

$$\left|\langle Cat|_\theta \cdot |Cat\rangle_{\text{Even}}\right|^2 = \left(\left(1 + \exp\left(-|\alpha_L|^2 - \alpha_L^* \alpha_L\right)\right) \cdot \left(1 + \mathrm{e}^{i\theta}\right)\right)^2 \sim 1 + \cos(\theta)$$

$$\left|\langle Cat|_\theta \cdot |Cat\rangle_{\text{Odd}}\right|^2 = \left(\left(1 - \exp\left(-|\alpha_L|^2 - \alpha_L^* \alpha_L\right)\right) \cdot \left(1 - \mathrm{e}^{i\theta}\right)\right)^2 \sim 1 - \cos(\theta)$$

In the equator plane of Bloch-sphere, the interferences have the form $1 \pm \cos(\theta)$; therefore, one can define the visibility $V = P_{Max} - P_{Min} / P_{Max} + P_{Min}$ to evaluate the coherence, where P is the corresponding detected power. The interference curves and visibilities for "kitten" and "cat" states are shown in Fig. 4 in the main text.

For an a-CS, the overlap between two opposite-amplitude a-CST is calculated by the correlation coefficient r,

$$r = \frac{\sum_x \sum_y \left(E_p - \bar{E}\right)\left(E_n - \bar{E}\right)}{\sqrt{\left(\sum_x \sum_y \left(E_p - \bar{E}\right)^2\right) \cdot \left(\sum_x \sum_y \left(E_n - \bar{E}\right)^2\right)}} \tag{S8}$$

where p and n signify positive ($\alpha_L > 0$) and negative ($\alpha_L < 0$) the a-CST; E_p, E_n, and $\bar{E}$ represent positive, negative, and average electric distributions, respectively. For an a-CS, the correlation coefficient is calculated (see Supplementary Table 1), where the overlap between two a-CSTs approaches zero when the size $|\alpha_L|$ is equal to $\sqrt{3.5}$. For this reason, the a-CS can be named as "kitten" when the $|\alpha_L|$ is smaller than $\sqrt{3.5}$.

Supplementary Note 4. Experimental results for wavefronts of the a-CS.

To study the wavefront of the a-CS, we study the interference between the sum of GILs and a referenced beam. Supplementary Figure 5 shows the setup, including a beam splitter (BS), a neutral attenuator (AT), and a CCD. In our setup, the distance is 0.8 m from SLM to convex lens F3, and 0.17m from F3 to the CCD, respectively. One of the paths, i.e., port A, refers to a referenced Gaussian beam expanded by a telescopic system, and the other (port B) is the a-CS with two GILs. The CCD is used to observe interference patterns in port C or D. Supplementary Figure 6 a-d show the theoretical interference patterns of the a-CSs from $\sqrt{0.5}$ to $\sqrt{5.0}$. Correspondingly, the experimental measurements registered by CCD are shown in Supplementary Figure 6e-h. The results indicate that two separated GILs have two genuine Gaussian wavefronts without any screw dislocation.

Supplementary Note 5. The details for state tomography.

In the process of state tomography, the mutually unbiased bases (MUBs) $\left\{\left|a_m^j\right\rangle\right\}$ in Hilbert space can be generated using the Weyl group, Hadamard matrix, and Fourier–Gauss transform methods. Here, we used the discrete Fourier–Gauss transform to product MUBs in prime space [6],

$$\left\{|\mathrm{a}_m^j>\right\} = \left\{\frac{1}{\sqrt{d}}\sum_{n=0}^{d-1}\omega_d^{\left(jn^2+nm\right)}|\mathrm{n}>\right\} = \left\{\frac{1}{\sqrt{d}}\sum_{n=0}^{d-1}e^{i\frac{2\pi}{d}(jn^2+nm)}|\mathrm{n}>\right\} \qquad \text{(S9)}$$

Where j indexes the group of the MUBs, $j=0\ldots d-1$; $m\ (=0\ldots d-1)$ indexes the superposed OAM states for each set in MUBs, and $\left|\left\langle a_m^j \middle| a_{m'}^{j'}\right\rangle\right|^2 = 1/d\left(1-\delta_{jj'}\right)$ for the MUBs. In actuality, j runs from 0 to d, with the last set of MUBs being the OAM eigenstates.

$$\left\{\left|a_m^d\right\rangle\right\} \to \left\{|0>,|1>,\ldots|d-1>\right\}.$$

For a two-dimensional OAM space (d=2), the eigenstates of three Pauli operators form a complete set of MUBs, which can be represented by the following three matrices:

$$\pi_1 = \begin{bmatrix}1 & 0\\ 0 & 1\end{bmatrix}; \pi_2 = \frac{1}{\sqrt{2}}\begin{bmatrix}1 & 1\\ 1 & -1\end{bmatrix}; \pi_3 = \frac{1}{\sqrt{2}}\begin{bmatrix}1 & 1\\ i & -i\end{bmatrix}.$$

The corresponding measured superposed OAM states are

$$\begin{aligned}
&\{\mathrm{I}_1\} = \left\{|0>,|1>\right\}\\
&\{\mathrm{I}_2\} = \left\{\frac{|0>+|1>}{\sqrt{2}}, \frac{|0>-|1>}{\sqrt{2}}\right\}\\
&\{\mathrm{I}_3\} = \left\{\frac{|0>+i|1>}{\sqrt{2}}, \frac{|0>-i|1>}{\sqrt{2}}\right\}
\end{aligned}$$

For higher dimensional space, we calculate these states using Eq. S9. From the theoretical and experimental measured distributions P_{jm}, one can determine the similarity that equals the fidelity [7,8].

$$S = \sum_{j,m}\sqrt{P_{jm}P'_{jm}} \Big/ \sum_{j,m}P_{jm}\sum_{j,m}P'_{jm} \qquad \text{(S10)}$$

Supplementary References

1 Allen, L., Beijersbergen, M. W., Spreeuw, R. & Woerdman, J. Orbital angular momentum of light and the transformation of Laguerre-Gaussian laser modes. *Phys. Rev. A* **45**, 8185 (1992).

2 Tipsmark, A. *Generation of optical coherent state superpositions for quantum information processing*, PhD thesis,Technical University of Denmark (DTU),Denmark, (2012).

3 Lvovsky, A. I. a. R., Michael G. Continuous-variable optical quantum-state tomography. *Rev. Mod. Phys.* **81**, 299 (2009).

4 Neergaard-Nielsen, J. S. *Generation of single photons and Schrödinger kitten states of light*, PhD thesis, University of Copenhagen, Denmark, (2008).

5 Björk, G. & Mana, P. G. L. A size criterion for macroscopic superposition states. *J. Opt. B: Quantum Semiclass. Opt.* **6**, 429 (2004).

6 Wieśniak, M., Paterek, T. & Zeilinger, A. Entanglement in mutually unbiased bases. *New J. Phys.* **13**, 053047 (2011).

7 Bolduc, E., Bent, N., Santamato, E., Karimi, E. & Boyd, R. W. Exact solution to simultaneous intensity and phase encryption with a single phase-only hologram. *Opt. Lett.* **38**, 3546-3549 (2013).

8 D'ambrosio, V. *et al.* Test of mutually unbiased bases for six-dimensional photonic quantum systems. *Sci. Rep.* **3**, 2726 (2013).